---

1. Question 1

   (1.1) The Routh array was constructed by first rewriting the characteristic equation of the closed-loop system using the substitution $T_I = \frac{1}{\tau_I}$ to simplify the algebra. The goal was to determine the range of K_C and τ_I values that lead to a stable system based on Routh-Hurwitz criteria.

Question 1 $\quad G_c = K_c + T_I \frac{1}{s} = \frac{K_c s + T_I}{s}$

1.1

$$\frac{Y(s)}{R(s)} = \frac{\frac{2}{s^3+4s^2+5s+2}\left(\frac{K_c s + T_I}{s}\right)}{1 + \frac{2}{s^3+4s^2+5s+2}\left(\frac{K_c s + T_I}{s}\right)}$$

$$= \frac{\frac{2K_c s + 2T_I}{s^4+4s^3+5s^2+2s}}{1 + \frac{2K_c s + 2T_I}{s^4+4s^3+5s^2+2s}}$$

$$= \frac{2K_c s + 2T_I}{(s^4+4s^3+5s^2+2s) + 2K_c s + 2T_I}$$

$$= \frac{2K_c s + 2T_I}{s^4+4s^3+5s^2+(2+2K_c)s+2T_I}$$

$$D(s) = s^4+4s^3+5s^2+(2+2K_c)s + 2T_I = 0$$

Routh Array

4	1	5	$2T_I$
3	4	$2+2K_c$	0
2	b_3	b_1	b_0
1	c_3	c_1	c_0
0	d_3	d_1	d_0

Figure 1: Step 1 of Routh Array derivation.

$$b_3 = -\frac{1}{4}\begin{vmatrix} 1 & 5 \\ 4 & 2+2K_c \end{vmatrix}$$

$$= -\frac{1}{4}\left[(2+2K_c) - 5(4)\right]$$

$$= -\frac{1}{2} - \frac{1}{2}K_c + 5$$

$$= 4.5 - \frac{1}{2}K_c$$

$$b_1 = -\frac{1}{4}\left(-4(2T_I)\right)$$

$$= 2T_I$$

$$b_0 = 0$$

$$c_3 = -\frac{1}{b_3}\left[4b_1 - (2+2K_c)b_3\right]$$

$$= \frac{-4b_1}{b_3} + (2+2K_c)$$

$$= \frac{-8T_I}{4.5 - \frac{1}{2}K_c} + 2 + 2K_c$$

$$c_1 = 0$$

$$c_0 = 0$$

$$d_3 = -\frac{1}{c_3}(-b_1 c_3)$$

$$= b_1$$

$$= 2T_I$$

$$d_1 = 0$$

$$d_0 = 0$$

Figure 2: Step 2 of Routh Array derivation.

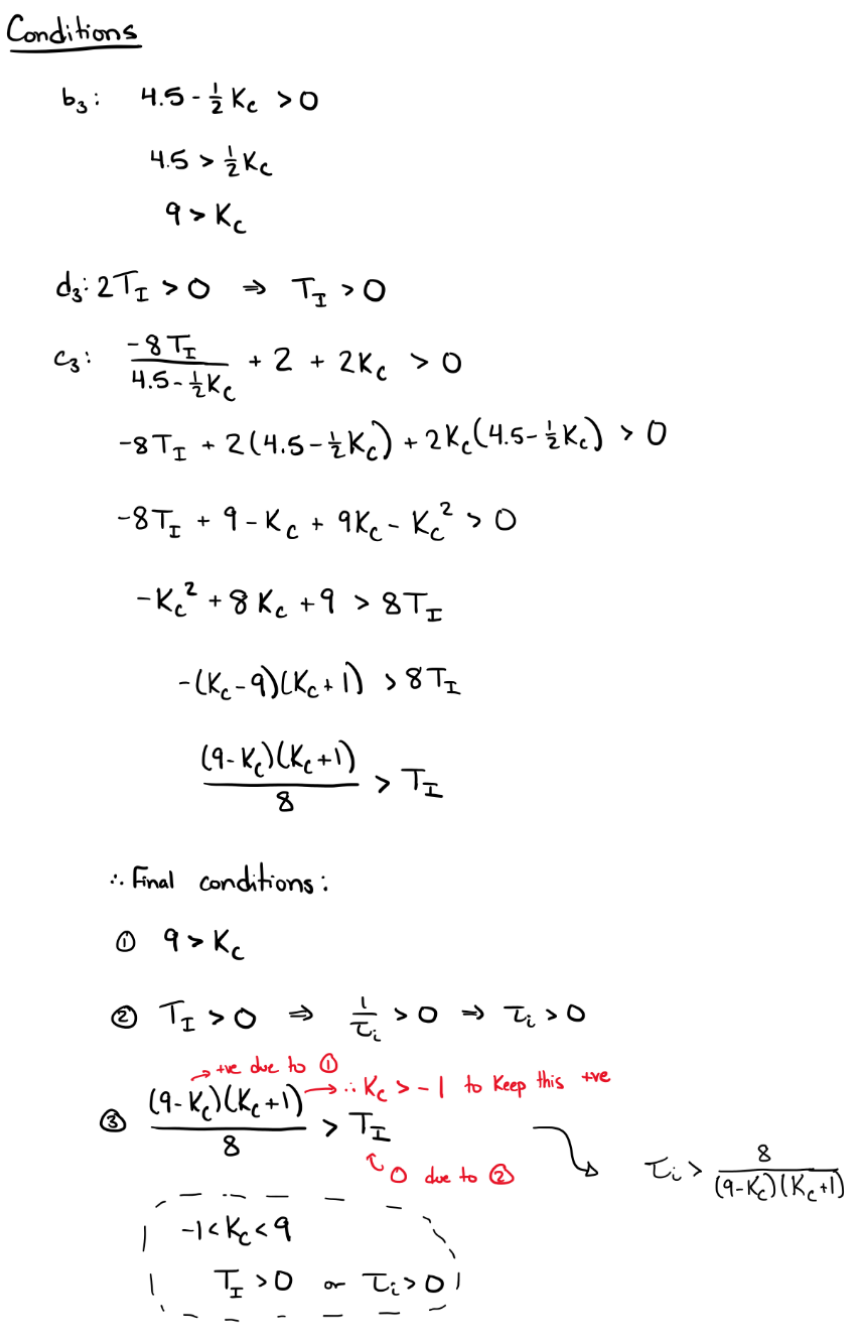

Figure 3: Final Routh Array with derived inequalities for stability.

(1.2) Using the inequalities derived in 1.1, the feasible set was plotted to visualize combinations of K_C and τ_I that result in closed-loop stability. The red shaded region indicates infeasible (unstable) parameter combinations.

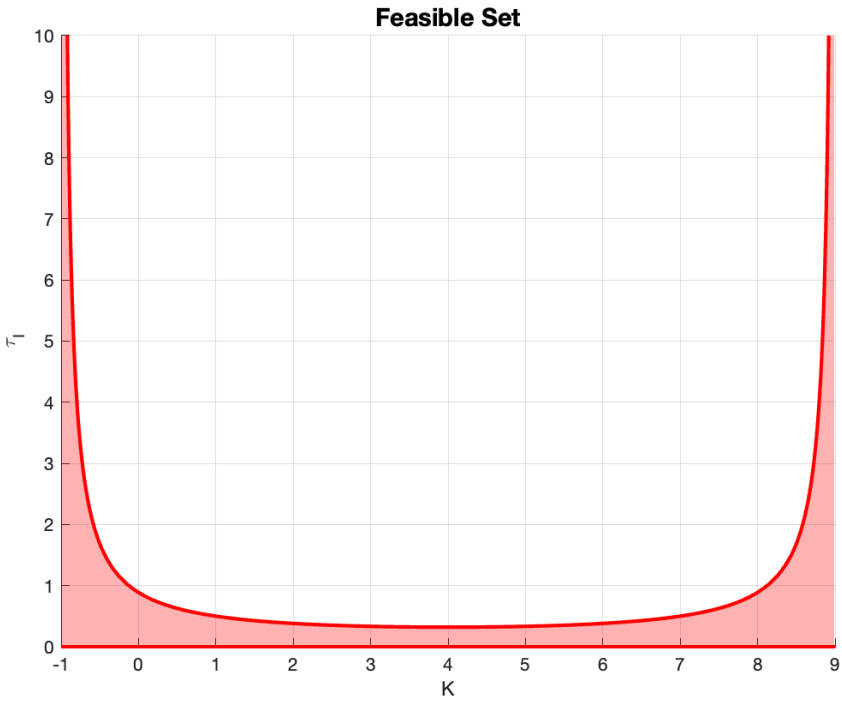

Figure 4: Feasible set for K_C and τ_I from Routh-Hurwitz conditions.

(1.3) A Simulink model was developed to simulate the closed-loop response of the system. Three scenarios were tested: one inside the feasible region, one outside, and one on the edge.

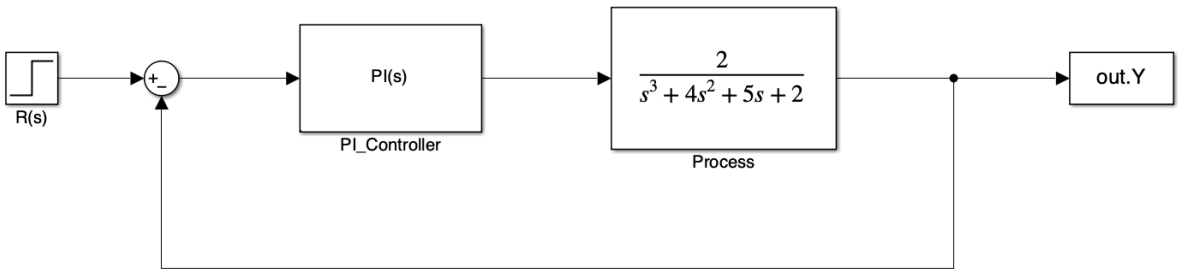

Figure 5: Simulink model of the PI-controlled system.

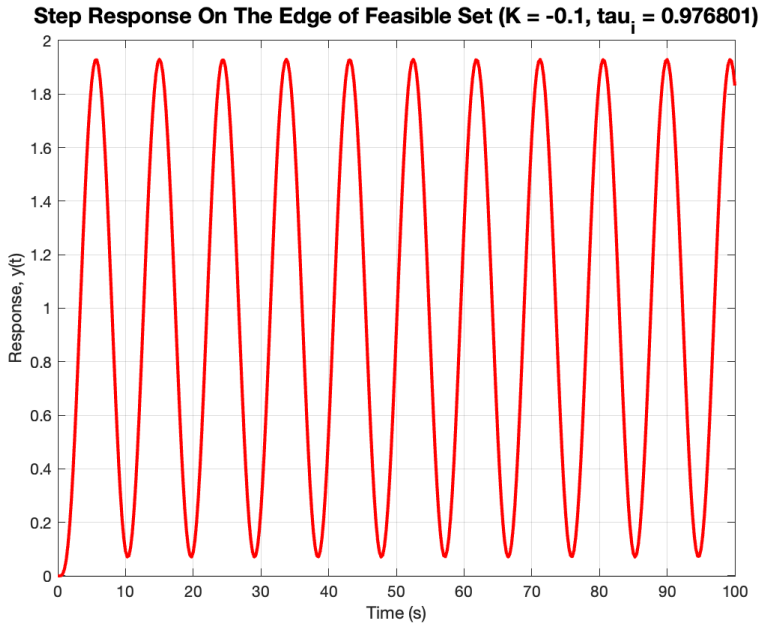

Figure 6: Step response on the boundary of the feasible set. The system oscillates and the amplitude grows very slowly, indicating marginal instability.

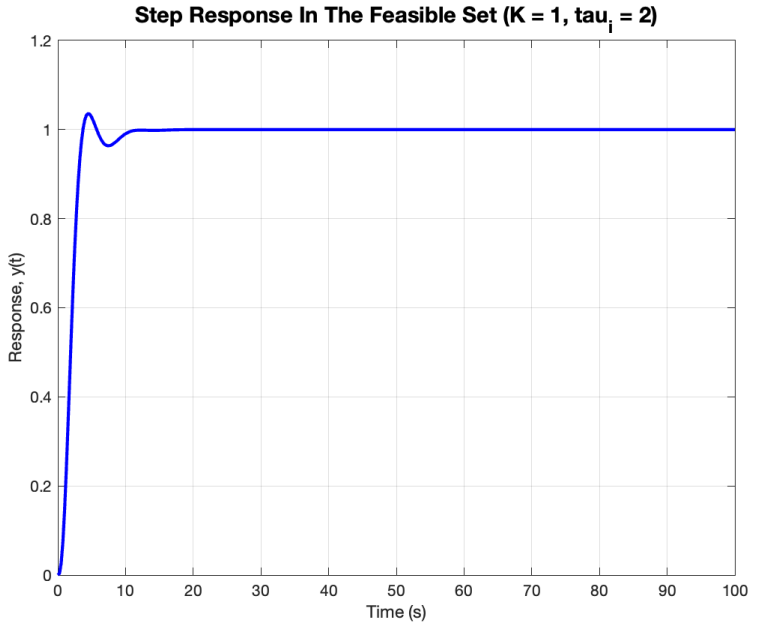

Figure 7: Step response for parameters inside the feasible set. The system is stable and relatively well damped, approaching steady state smoothly.

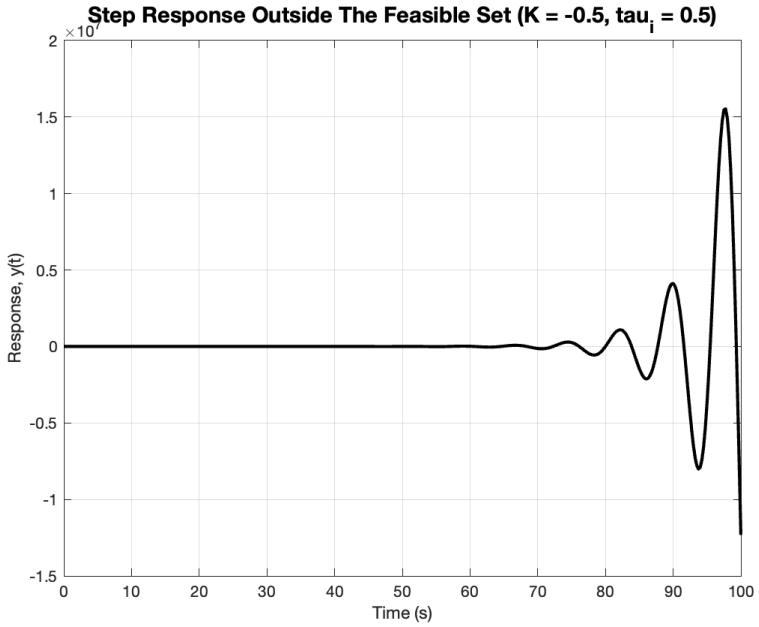

Figure 8: Step response for parameters outside the feasible set. The system exhibits fast-growing oscillations, clearly demonstrating instability.

The edge case exhibits slow-growing oscillations, which indicates marginal instability. Although the system initially appears to behave stably, the oscillations increase in amplitude over time. This is consistent with the fact that the chosen parameters lie directly on the boundary of the feasible set, where the Routh-Hurwitz conditions require strict inequalities ($>$) rather than allowing equality. The second case, which is well within the feasible region, produces a stable and mostly well-damped response. The final case, with parameters outside the feasible set, immediately shows rapidly growing oscillations, confirming instability.

(1.4) The Routh-Hurwitz array was recomputed with the new transport delay (using first-order Padé approximation) to determine how the delay affects system stability.

1.4

$$G_c = K_c + T_I\frac{1}{s} = \frac{K_c s + T_I}{s} \qquad G_M = e^{-0.5s} \approx \frac{1-0.25s}{1+0.25s}$$

$$\frac{Y(s)}{R(s)} = \frac{\frac{2}{s^3+4s^2+5s+2}\left(\frac{K_c s+T_I}{s}\right)}{1+\frac{2}{s^3+4s^2+5s+2}\left(\frac{K_c s+T_I}{s}\right)\left(\frac{1-0.25s}{1+0.25s}\right)}$$

$$= \frac{(2K_c s + 2T_I)(1+0.25s)}{(s^4+4s^3+5s^2+2s)(1+0.25s) + (2K_c s+2T_I)(1-0.25s)}$$

$$= \frac{2K_c s + 2T_I + 0.5K_c s^2 + 0.5T_I s}{s^4+4s^3+5s^2+2s+0.25s^5+s^4+\frac{5}{4}s^3+0.5s^2+2K_c s+2T_I-0.5K_c s^2-0.5T_I s}$$

$$= \frac{0.5K_c s^2 + (2K_c+0.5T_I)s + 2T_I}{0.25s^5+2s^4+\frac{21}{4}s^3+(5.5-0.5K_c)s^2+(2+2K_c-0.5T_I)s+2T_I}$$

$$D(s) = 0.25s^5+2s^4+\frac{21}{4}s^3+(5.5-0.5K_c)s^2+(2+2K_c-0.5T_I)s+2T_I = 0$$

Routh Array

5	0.25	$\frac{21}{4}$	$2+2K_c-0.5T_I$
4	2	$5.5-0.5K_c$	$2T_I$
3	b_4	b_2	b_0
2	c_4	c_2	c_0
1	d_4	d_2	d_0
0	e_4	e_2	e_0

Figure 9: Step 1 of Routh Array with transport delay.

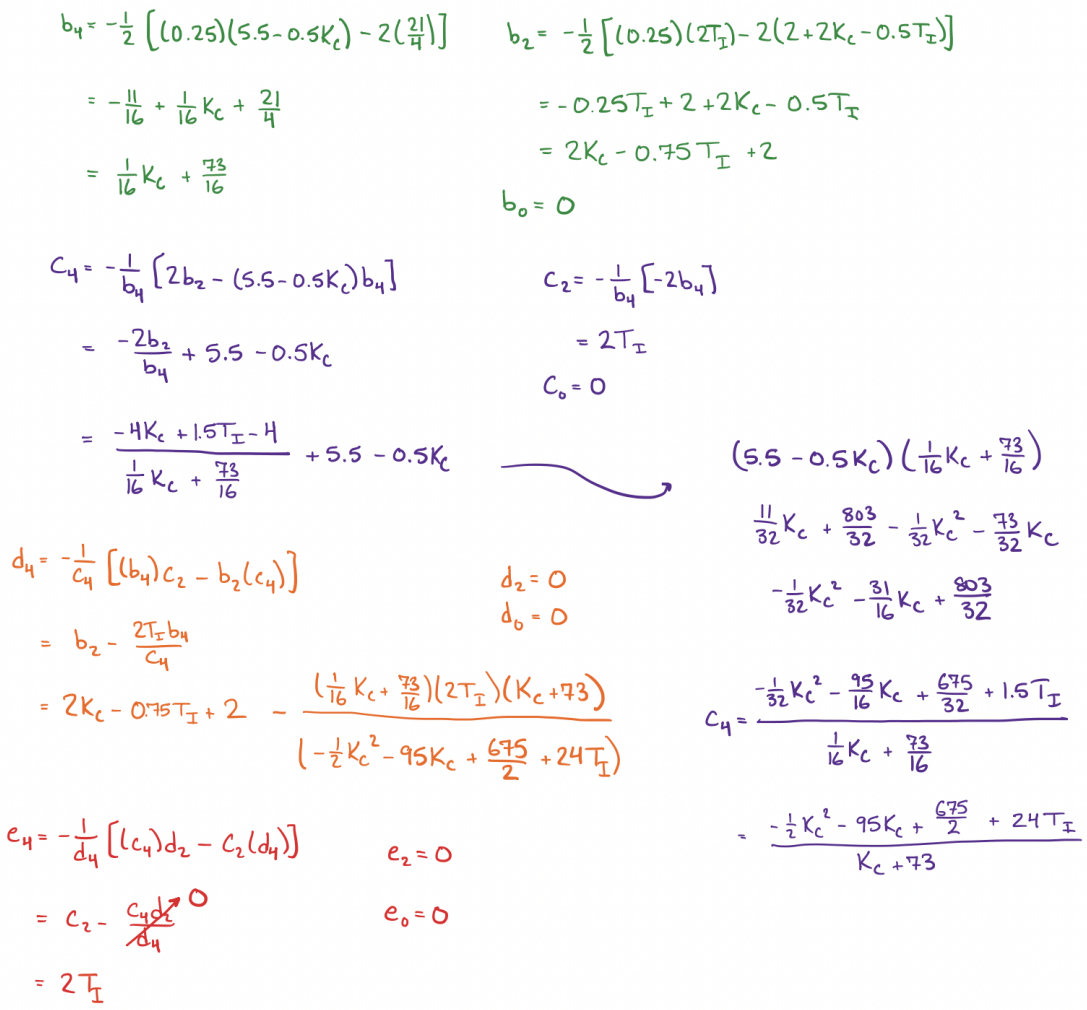

Figure 10: Step 2 of Routh Array with transport delay.

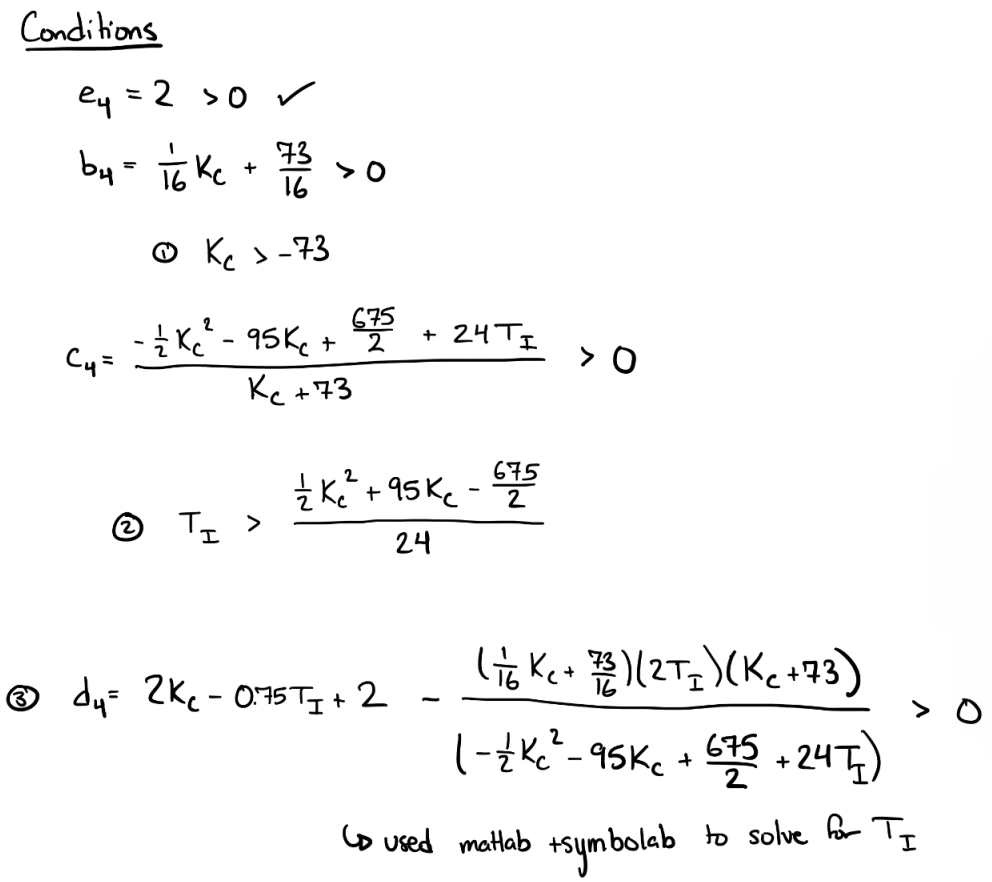

Figure 11: Final Routh Array with delay-based conditions.

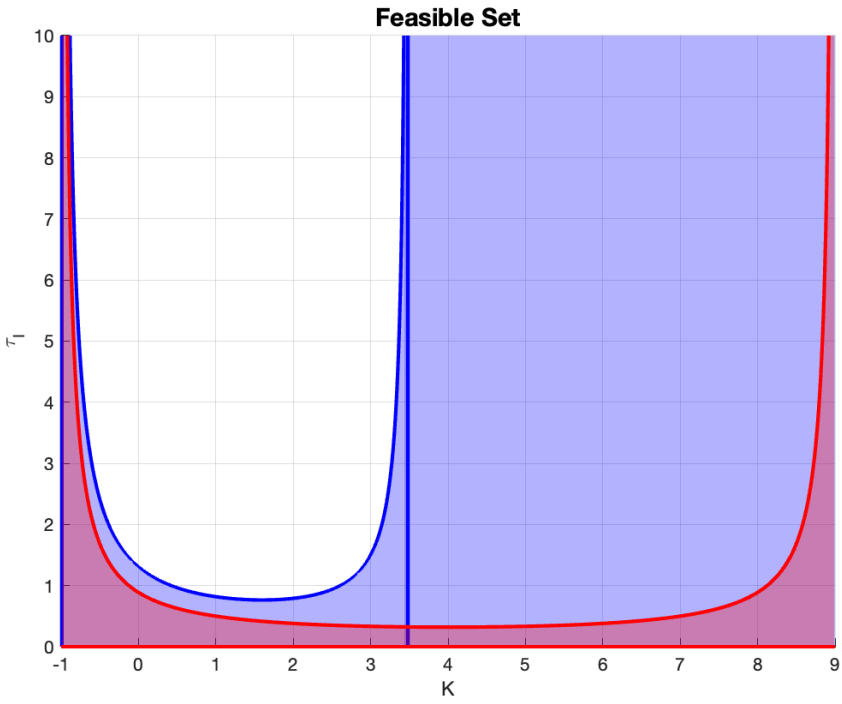

Figure 12: Feasible sets with and without delay. Blue indicates infeasible region of the new delayed system. Red is the same infeasible region from earlier.

As seen in the figure, the introduction of transport delay reduces the size of the feasible region, particularly in areas with small integral time τ_I or large controller gain K_C. This is because transport delay introduces additional phase lag into the system, which decreases the phase margin and brings the system closer to instability. From the perspective of the Bode plot, delay shifts the phase curve to the left, meaning that the phase crosses $-180°$ at a lower frequency. This corresponds to a higher critical gain A_c, which implies a lower allowable K_C for stability. In practical terms, this means that the system must be detuned (K_C must be reduced) when delay is present. If the gain is not reduced accordingly, the aggressive controller action causes excessive oscillations, and the system approaches instability. This explains why many of the previously stable combinations of K_C and τ_I now fall outside the feasible set when delay is introduced.

(1.5) The system was simulated again using the same controller parameters ($K_C = 2$, $\tau_I = 1$) for both the delay and non-delay versions. These values were chosen by looking at the feasible sets and picking values that lay in both the time delay and non-delay feasible sets. The updated Simulink model includes the transport delay block.

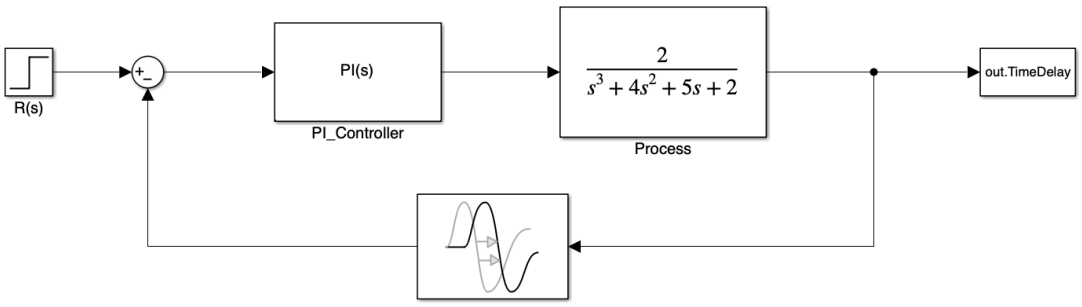

Figure 13: Simulink model with transport delay included.

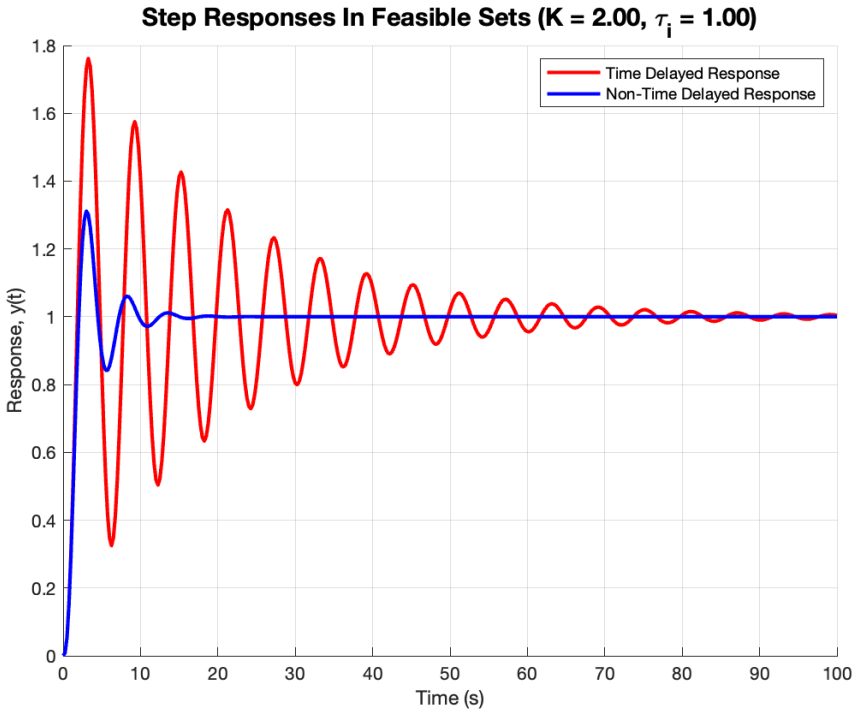

Figure 14: Comparison of system response with and without transport delay.

The system with transport delay exhibits more oscillatory behavior and takes longer to settle compared to the delay-free case, despite using identical PI tuning parameters. This aligns with the analysis in 1.4, where the added phase lag from delay was shown to reduce stability margins and narrow the feasible set. The delay effectively pushes the system closer to instability, and without detuning K_C, even stable configurations become more oscillatory and sluggish in response.

2. Question 2

(2.1) The approximated first-order system equation for the closed-loop system is given by:

$$\frac{Y(s)}{U(s)} = \frac{-1.2e^{-5s}}{6s+1} = \frac{Ke^{-\theta s}}{\tau s+1} \tag{1}$$

We first start with the **Cohen-Coon** heuristic. From class, we are given the following equations:

$$K_C = \frac{1}{K}\cdot\frac{\tau}{\theta}\left(\frac{4}{3}+\frac{\theta}{4\tau}\right) \qquad \tau_I = \theta\cdot\frac{32+\frac{6\theta}{\tau}}{13+\frac{8\theta}{\tau}} \qquad K_D = \theta\cdot\frac{4}{11+\frac{2\theta}{\tau}}$$

We thus get the answers below:

$$K_c = \frac{1}{(-1.2)}\left(\frac{6}{5}\right)\left(\frac{4}{3}+\frac{5}{4\cdot 6}\right) = -1.54166$$

$$\tau_I = (5)\cdot\frac{32+\frac{6(5)}{(6)}}{13+\frac{8(5)}{(6)}} = 9.40677$$

$$K_D = (5)\cdot\frac{4}{11+\frac{2(5)}{(6)}} = 1.5789$$

We then move onto the **Ciancone** heuristic. Since this system is for setpoint tracking, we use the correlation graphs as shown in class. To avoid wasting digital ink, the graphs were not attached.

For all graphs, we need to derive the fraction dead time first:

$$\frac{\theta}{\theta+\tau} = \frac{5}{5+6} = 0.454545$$

For the graphs K_cK_p, $\frac{\tau_I}{\theta+\tau}$, and $\frac{K_D}{\theta+\tau}$, we get the values 0.73, 0.73, and 0.08 respectively. Solving for K_c, τ_I, and K_D gives us:

$$K_C = \frac{0.73}{-1.2} = -0.683 \qquad \tau_I = (5+6)\cdot 0.73 = 8.03 \qquad K_D = (5+6)\cdot 0.08 = 0.88$$

Lastly, we calculate the **ITAE** heuristic. We start with the equation:

$$Y = A\left(\frac{\theta}{\tau}\right)^B$$

The values of A and B are given in the table below:

Controller	**Mode**	**A**	**B**
PID	P	0.965	-0.85
	I	0.796	-0.1465
	D	0.308	0.929

Table 1: Controller Parameters A and B for PID Mode

We also note the following equations to calculate the parameters in set-point tracking:

$$Y_P = KK_C \qquad Y_I = \frac{\tau}{\tau_I} = A + B\left(\frac{\theta}{\tau}\right) \qquad Y_D = \frac{K_D}{\tau}$$

We do some mathematics:

$$Y_P = (0.965)\left(\frac{\theta}{\tau}\right)^{-0.85} = 1.12675 \qquad K_C = \frac{1.12675}{-1.2} = -0.938958$$

$$Y_I = (0.796) + (-0.1465)\cdot\left(\frac{\theta}{\tau}\right) = 0.67391 \qquad \tau_I = \frac{6}{0.67391} = 8.895$$

$$Y_D = (0.308)\left(\frac{\theta}{\tau}\right)^{0.929} = 0.26001 \qquad K_D = 0.26001 \cdot 6 = 1.56006$$

(2.2) The Bode plot is shown below in Figure 15.

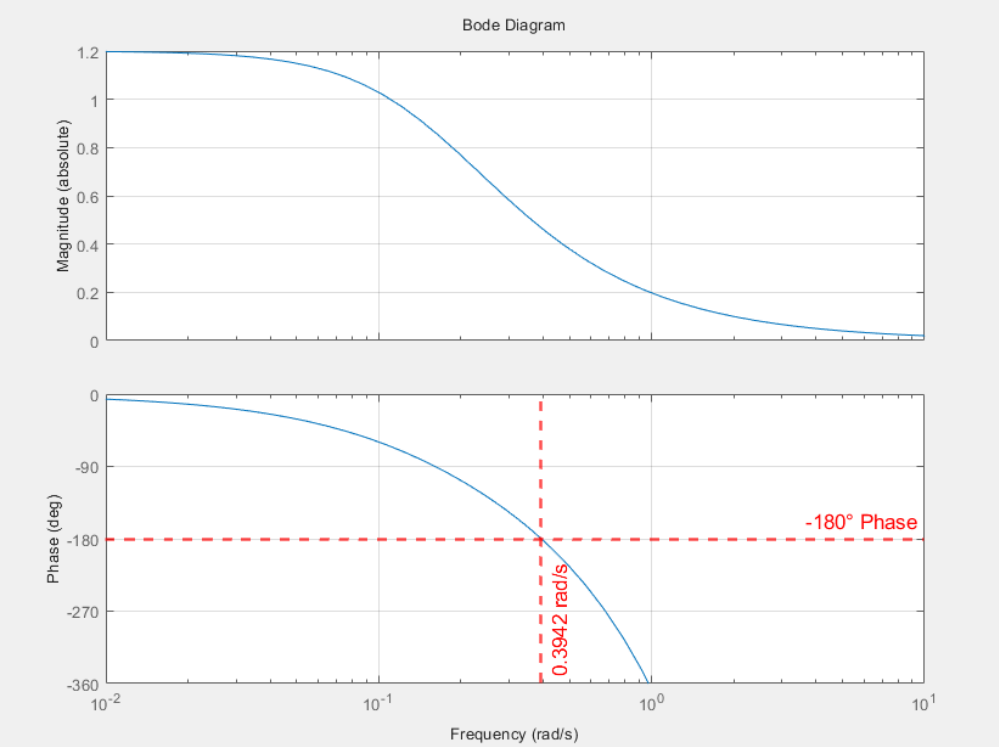

Figure 15: Bode plot of the closed-loop system with transport delay.

From the Bode plot and the associated Matlab code, we derive the Critical Frequency and the amplitude at said frequency as 0.3942 rad/s and 0.4673. With these numbers, we calculate the ultimate gain and the ultimate period.

$$K_u = \frac{1}{\text{Critical Amplitude}} = \frac{1}{0.3942} \approx 2.537$$

$$T_u = \frac{2\pi}{\omega_c} = \frac{2\pi}{0.4673} \approx 13.445$$

We then calculate the PID parameters K_c, τ_I and K_D using the Ziegler-Nichols tuning rules.

$$K_c = \frac{-K_u}{1.7} = \frac{-2.537}{1.7} \approx -1.492$$

$$\tau_I = \frac{T_u}{2} = \frac{13.445}{2} \approx 6.7225$$

$$K_D = \frac{T_u}{8} = \frac{13.445}{8} \approx 1.6806$$

(2.3) Looking at the Figure 16 and Figure 20, the Cohen-Coon controller exhibits a more aggressive and sharp transition. Its initial decrease is steeper and reaches a larger negative value compared to the other controllers. This behavior is likely

due to the high values of K_p and K_d within the controller. Additionally, the Cohen-Coon controller takes the longest time to converge, requiring close to 70 hours to stabilize.

In contrast, the Ciancone controller Figure 17 produces an output that resembles an overdamped response. While it is slower to converge compared to the ITAE and Ziegler-Nichols controllers, it is still faster than the Cohen-Coon controller, stabilizing in approximately 40 hours.

The ITAE controller (Figure 18) stands out for its faster convergence and smaller overshoot compared to the other designs. Its response is smooth and stable, making it an efficient choice.

The Ziegler-Nichols controller (Figure 19)follows a similar shape to the ITAE controller but exhibits a greater overshoot and more pronounced oscillations.

Based on the analysis of all the graphs, the ITAE controller demonstrates the best overall performance among the four designs, offering a balance of speed, stability, and minimal overshoot.

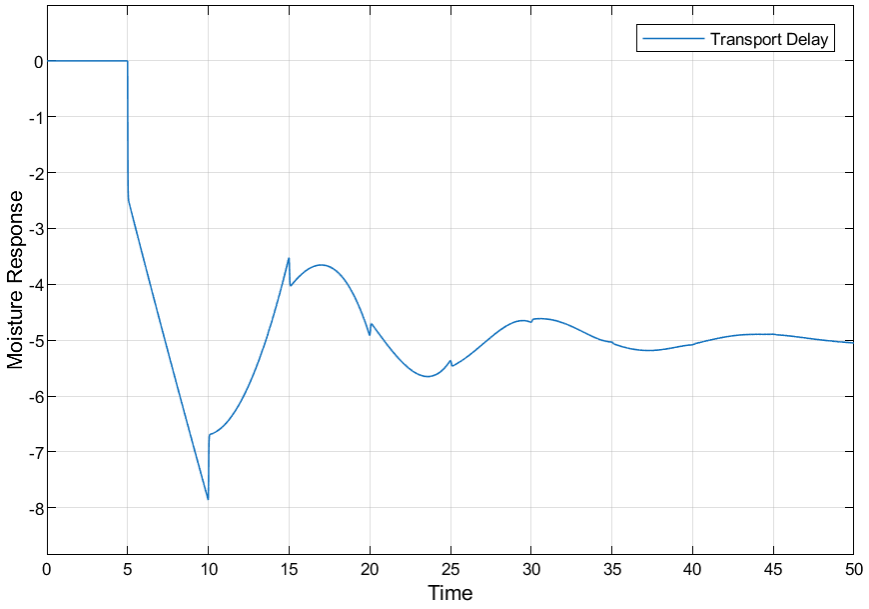

Figure 16: Step Response with Cohen-Coon Tuning

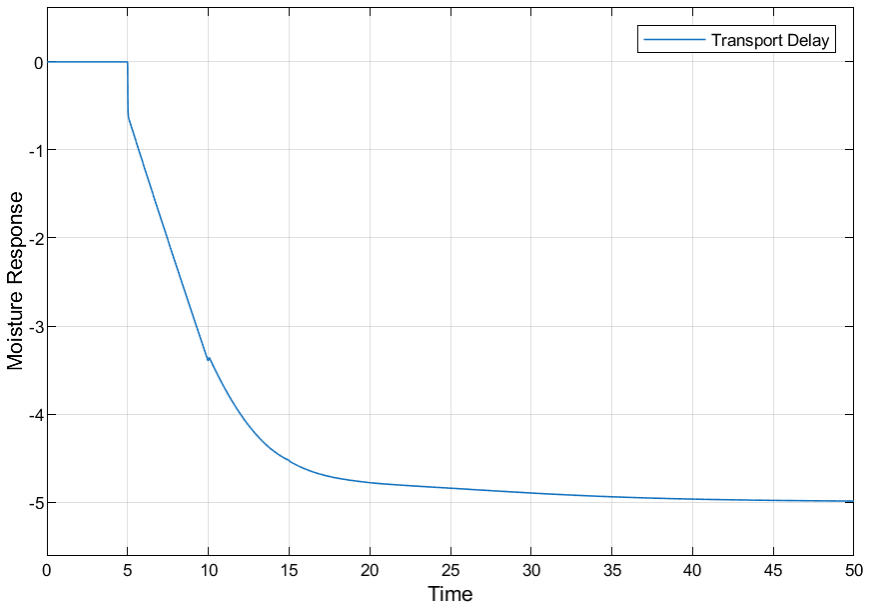

Figure 17: Step Response with Ciancone Tuning

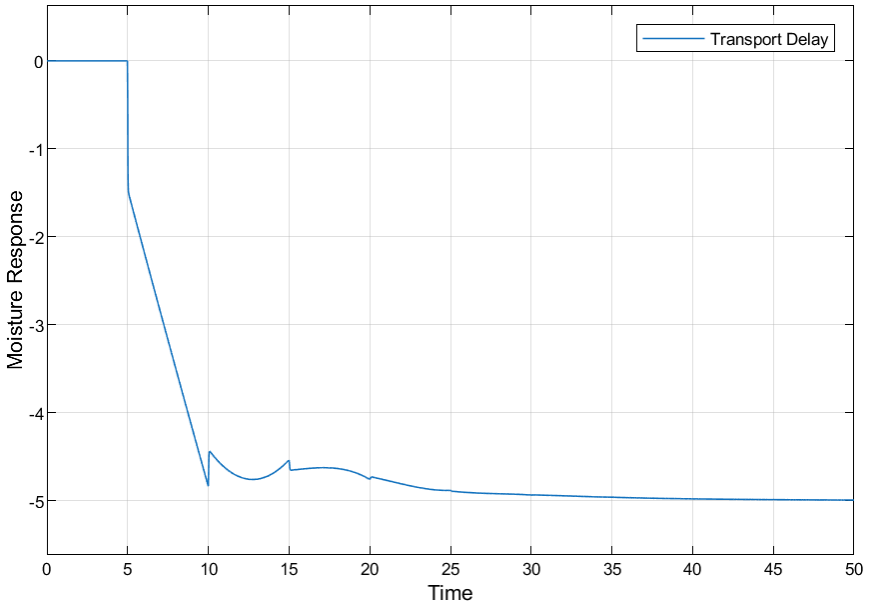

Figure 18: Step Response with ITAE Tuning

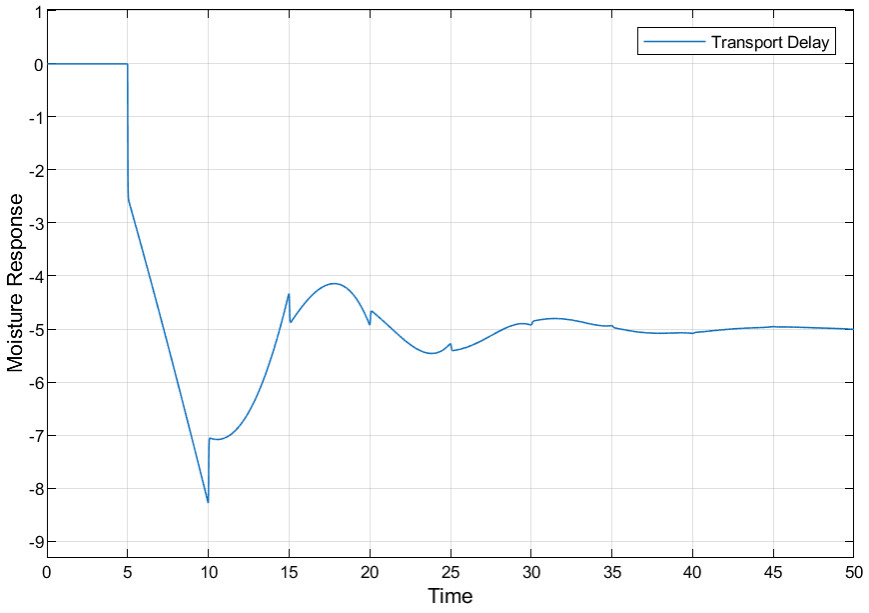

Figure 19: Step Response with Ziegler-Nichols Tuning

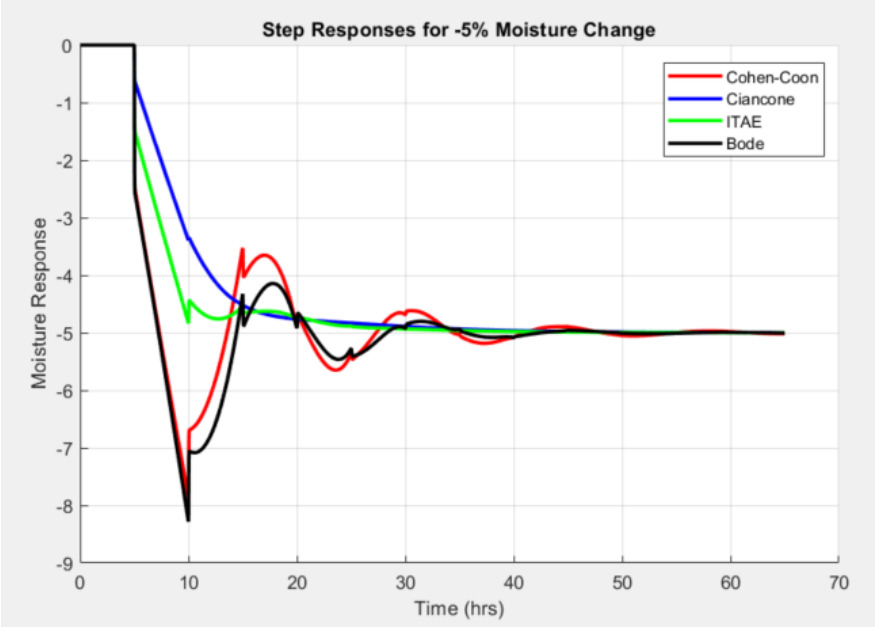

Figure 20: Comparison of Step Response with All Tuning

(2.4) To optimize the PID controller parameters, the derivative gain (K_d) was fixed at the ITAE value of $K_d = 1.56006$, while the proportional gain (K_c) and integral time (τ_I) were varied. Given our values from questions 2.1 and 2.2, we have a range of potential optimal proportional for the system. The values are shown below.

Controller	K_c	τ_I	K_d
Cohen-Coon	-1.54166	9.40677	1.5789
Ciancone	-0.683	8.03	0.88
ITAE	-0.938958	8.895	1.56006
Bode	-1.492	6.7225	1.6806

Table 2: Summary of PID Controller Parameters and Performance.

To visualize the performance of all the different initially-tuned controllers over the range of their parameters, we select to graph the contour plot over the range of $\{-1.7, -0.5\}$ for K_c and $\{5, 10\}$, which includes all the tuned parameters as well as a little arbitrary wiggle room on either side for both parameters. The system was simulated for a step change of -5% moisture, and the Integral Squared Error (ISE) was calculated for each combination of K_c and τ_I.

Figure 21 shows the contour plot of ISE values versus K_c and τ_I. The plot reveals a clear region of optimal performance, where the ISE is minimized. The optimal parameters were identified as:

$$K_c = -1.2, \quad \tau_I = 9$$

These values correspond to the lowest ISE, indicating the best controller performance in terms of minimizing overshoot, oscillations, and settling time – basically minimal large errors.

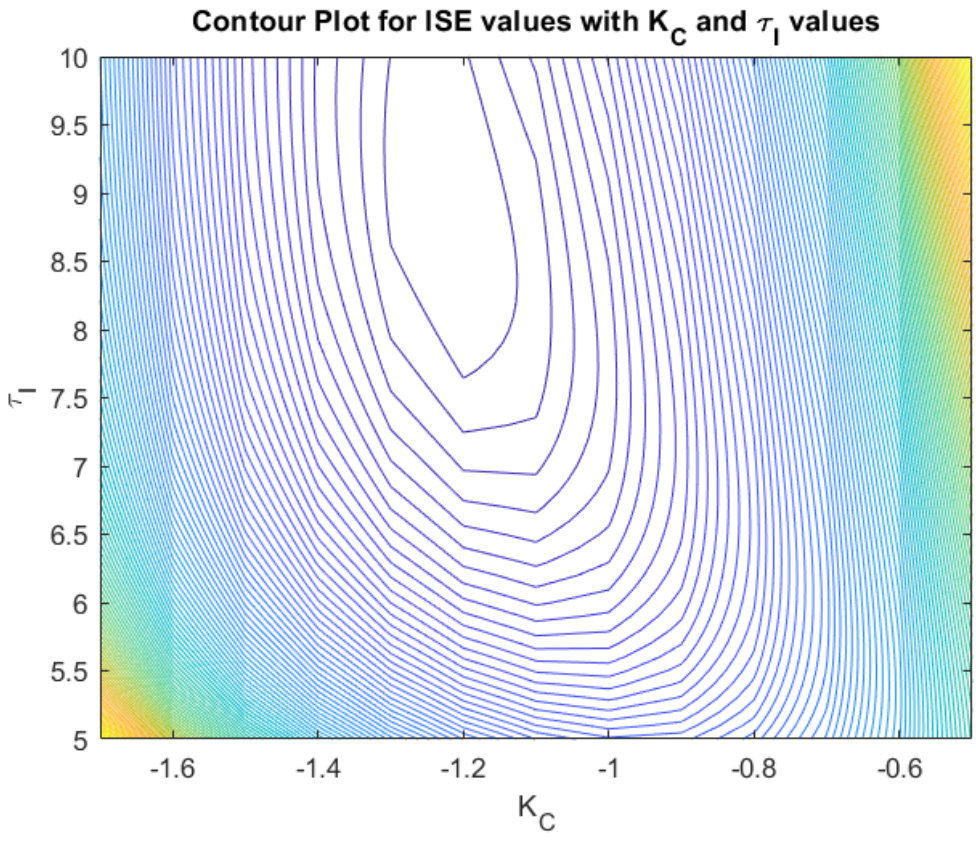

Figure 21: Contour Plot of ISE Values for Range of K_c and τ_I

The system was simulated with the optimal controller and compared to other designs, including Cohen-Coon, Ciancone, ITAE, and Bode controllers. Figure 22 shows the step responses for all controllers.

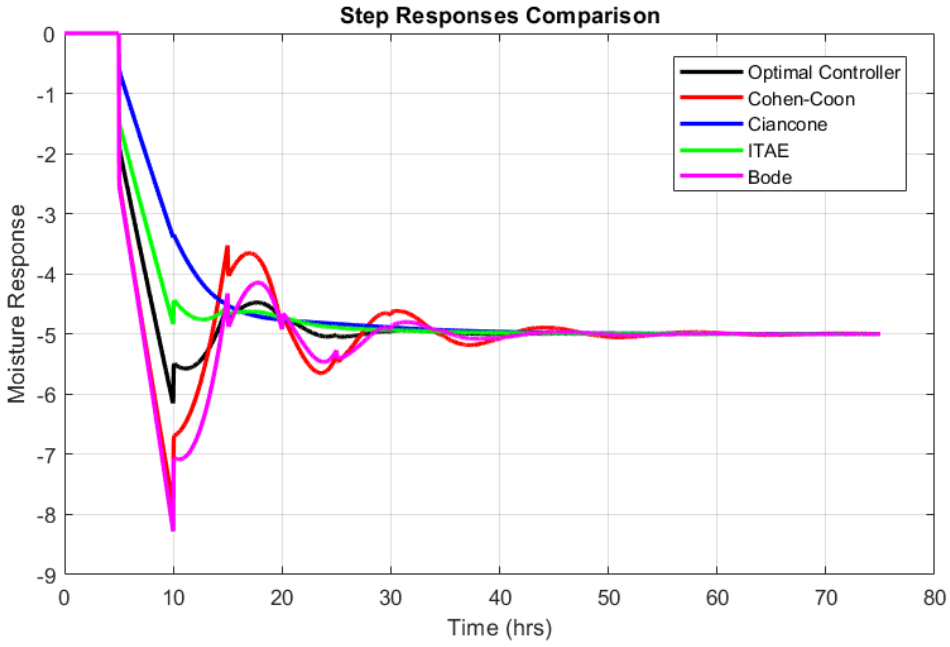

Figure 22: Contour Plot of ISE Values for Range of K_c and τ_I

Referring to 22, we can see that the optimal controller with minimal ISE has minimal overshoot, minimal settling time and the perfect amount of aggressiveness. Adding the final

Controller	K_c	τ_I	K_d
Cohen-Coon	-1.54166	9.40677	1.5789
Ciancone	-0.683	8.03	0.88
ITAE	-0.938958	8.895	1.56006
Bode	-1.492	6.7225	1.6806
Optimal	**-1.2**	**9**	**1.56006**

Table 3: Summary of PID Controller with Optimal Controller Parameters and Performance.

Note that the two closest controllers in K_c and τ_I are the ITAE and Cohen-Coon controllers, showing that their implementation in this scenario is closest to the optimal parameters given that K_D is selected as the K_D from the ITAE controller. A reason why those controllers might have the closest paramters to the optimal controller could be due to the K_D chosen being very similar to the Cohen-Coon K_D and literally the same thing as the ITAE K_D.